

Majorana corner pairs in a two-dimensional s -wave cold atomic superfluid

Ya-Jie Wu,^{1,2} Xi-Wang Luo,¹ Junpeng Hou,¹ and Chuanwei Zhang^{1,*}

¹*Department of Physics, The University of Texas at Dallas, Richardson, Texas 75080-3021, USA*

²*School of Science, Xi'an Technological University, Xi'an 710032, China*

We propose a method to prepare Majorana pairs at the corners of imprinted defects on a two-dimensional cold atom optical lattice with s -wave superfluid pairing. Different from previous proposals that manipulate the effective Dirac masses, our scheme relies on the sign flip of the spin-orbit coupling at the corners, which can be tuned in experiments by adjusting the angle of incident Raman lasers. The Majorana corner pairs are found to be located at the interface between two regimes with opposite spin orbit coupling strengths in an anticlockwise direction and are robust against certain symmetry-persevered perturbations. Our work provides a new way for implementing and manipulating Majorana pairs with existing cold-atom techniques.

I. INTRODUCTION

Majorana zero modes (MZMs) have attracted great attention in past decades owing to their non-Abelian exchange statistics and potential applications as topologically protected qubits [1, 2]. They also exhibit significant physics in a range of disciplines such as nuclear and particle physics [3]. Strenuous efforts to search for MZMs are underway in both theories and experiments. In recent years, a variety of schemes to realize Majorana excitations have been proposed [4–18] by utilizing p -wave superconductors (SCs) or superfluid (SFs) [4, 5], or SCs and SFs with effective p -wave pairing via spin-orbit coupling (SOC) and s -wave pairing [6–10]. Remarkable experimental progresses have been made in condensed-matter systems [19–24]. The experimental realization of SOC in ultracold atomic gases offer another clean platform to explore Majorana physics [25–31]. In these platforms, the interplay among SOC, Zeeman fields and s -wave interactions could produce non-Abelian topological superfluids (TSFs) that host Majorana excitations. There have been several tantalizing proposals for realizing and tuning Majorana excitations, for example, by creating topological defects (such as SF vortices or lattice dislocations) or defect chain [32, 33].

The emergence of Majorana excitations can be intuitively understood by the low-energy theory. A pair of MZMs exist at the kinks where the pairing potential or SOC changes the sign (which corresponds to the sign change of Dirac mass or velocity in Jackiw–Rebbi model). In solid-state materials, the SOC kinks are difficult to tune, while the kinks of pairing potentials can be realized through Josephson junctions in superconducting nanowires, as well as the corners and hinges in recently proposed higher-order topological SCs (TSCs) [34–46]. In particular, for two-dimensional (2D) second-order TSCs, the bulk topology of the 2D system offers 1D edge modes, which have different topologies for adjacent edges due to the change of the pairing sign, leading to zero-

energy Majorana Kramers pairs or Majorana modes at corners [42–45]. On the other hand, in cold atomic system, the kinks of pairing potentials may be obtained by soliton excitations [47, 48]. However, these cold atomic systems suffer from dynamical instability in the presence of perturbations. Thus, proposals for realizing robust MZMs in atomic systems, through other manners like SOC kinks, are highly in demand.

In this paper, we propose feasible schemes to realize SOC kinks using trapped ultracold fermionic atoms on a 2D optical lattice, and show that our system supports Majorana pairs in a vortex-free configuration. The main results are listed below:

(i) Effective 1D modes on a rectangular geometry would emerge in the 2D system through engineering on-site potential of the rectangle. In the presence of 1D equal Rashba-Dreeshauls (ERD) SOC, Majorana corner pair emerges at the corner of the rectangle with a proper s -wave pairing.

(ii) Each edge of the rectangular defect is characterized by a 1D topological SF in the BDI class, and Majorana pair exists at the interface of two adjacent edges which have different signs of SOC (clockwise or anticlockwise along the defective geometry). Our system is in analog with the higher-order TSCs except that the low-energy 1D model is induced by the defect rectangle rather than the bulk topology, and the MZMs are induced by SOC kinks rather than pairing kinks between two adjacent boundaries [42, 43]. Our system is more concise and experimentally friendly since no tricky unconventional pairings like d -wave or s_{\pm} -wave are required.

(iii) Our system can be realized with currently already established experimental techniques in cold atoms, including 1D ERD SOC by Raman lasers [25, 26], single-site addressing in 2D optical lattices [49–53], and tunable s -wave interaction through Feshbach resonance [54, 55].

(iv) The Majorana corner pair is robust against shape deformation of the defective rectangle, even to the extent of a defective loop. In addition, the SOC direction dictates on which corners the Majorana pair resides. Therefore the incident direction of Raman lasers can be used to manipulate the Majorana pairs.

The paper is organized as follows. In Sec. II we first

*chuanwei.zhang@utdallas.edu

introduce the Hamiltonian with 1D ERD SOC on optical lattices, and obtain the phase diagram consisting of metal and s -wave SF phases. In Sec. III, we study the case with a defective rectangle, and find Majorana pairs emerge at the corners. We extend the discussion to a ring-shaped geometry in Sec. IV, where the Majorana pairs arise naturally due to soft domain walls of SOC. Finally, we make conclusions and discussions in Sec. V.

II. SPIN-ORBIT-COUPLED s -WAVE SUPERFLUIDS ON 2D OPTICAL LATTICES

We utilize atomic hyperfine states as the pseudospin states $|\uparrow\rangle$ and $|\downarrow\rangle$, as illustrated in Fig. 1. The SOC is synthesized by two counter-propagating Raman lasers coupling the two hyperfine states. The single atom motion in 2D real space is described by the Hamiltonian $\hat{H}_{0,a} = \frac{\vec{k}^2}{2m_0} + \frac{\delta}{2}\sigma_z + (\Omega e^{2i\vec{k}_0 \cdot \vec{r}} |\downarrow\rangle \langle\uparrow| + h.c.)$, where the reduced Planck constant \hbar has been set to be 1, $\Omega \propto \Omega_1 \Omega_2^*$ is the strength of Raman coupling, and $\vec{k}_0 = k_{0,x}\vec{e}_x + k_{0,y}\vec{e}_y$ is the wave vector of the Raman laser. The off-diagonal terms correspond to a spin flip process accompanied by a momentum transfer of $2\vec{k}_0$, describing the SOC effects. The detuning term reads $\delta = \omega_z - \delta\omega$, where $\omega_z > 0$ is the energy difference between these two hyperfine states, and $\delta\omega$ denotes the frequency difference between two Raman laser beams. In the following, we assume that other hyperfine levels are far off-resonance under the two-phonon process, for example, by quadratic Zeeman shift. The Hamiltonian is first transformed by a unitary matrix, namely, $\hat{H}_{0,b} = U\hat{H}_{0,a}U^{-1}$, where $U = \text{diag}(e^{-i\vec{k}_0 \cdot \vec{r}}, e^{i\vec{k}_0 \cdot \vec{r}})$. We then perform another pseudo-spin rotations $\tilde{U} = e^{-i\frac{\pi}{4}\sigma_z} e^{-i\frac{\pi}{4}\sigma_y}$ to obtain $\hat{H}_0 = \tilde{U}\hat{H}_{0,b}\tilde{U}^\dagger$, which can be written as

$$\hat{H}_0 = \frac{1}{2m_0} \left[(k_x + k_{0,x}\sigma_y)^2 + (k_y + k_{0,y}\sigma_y)^2 \right] + \frac{\delta}{2}\sigma_y - \Omega\sigma_z. \quad (1)$$

The Raman transition produces a desired ERD SOC. In the following, we assume $\delta = 0$ for convenience.

1D system suffers from strong quantum fluctuations, which could eliminate s -wave SF order, together with the Majorana modes. This motivates us to investigate the physics in 2D, where quasi-long-range SF order exists below the Berezinskii-Kosterlitz-Thouless (BKT) transition temperature. We concentrate on the lowest (nearly) degenerate bands for constructing a tight-binding model. From Eq. (1), through the operator $\hat{\Psi}(\vec{r}) = \sum_{i,\sigma} \hat{c}_{i,\sigma} \psi_\sigma(\vec{r} - \vec{r}_i)$ with $\psi_\sigma(\vec{r} - \vec{r}_i)$ the Wannier function at site i , we obtain a second-quantization formula:

$$\hat{H}_{0s} = \sum_i \left(-t_x \hat{c}_i^\dagger \hat{c}_{i+e_x} - t_y \hat{c}_i^\dagger \hat{c}_{i+e_y} - it_{sox} \hat{c}_i^\dagger \sigma_y \hat{c}_{i+e_x} - it_{soy} \hat{c}_i^\dagger \sigma_y \hat{c}_{i+e_y} \right) + h.c. - h_z \hat{c}_i^\dagger \sigma_z \hat{c}_i - \mu \hat{c}_i^\dagger \hat{c}_i, \quad (2)$$

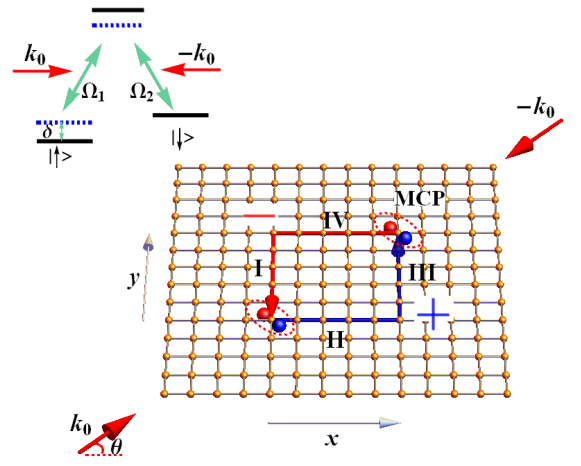


FIG. 1: Illustration of system setup on a 2D optical lattice, where two counter propagating Raman beams are incident with angle θ . A dip potential is applied on a rectangle geometry (indicated by the blue and red curves) through single-site addressing. Under the configuration $\theta = \pi/4$, the sign of effective SOC is positive (+)/negative (-) on the blue/red lines in edge coordinate along the arrows. Two spheres (encircled by the red dashed oval) at the interface denote the Majorana corner pair (MCP). The inset above shows the level diagram.

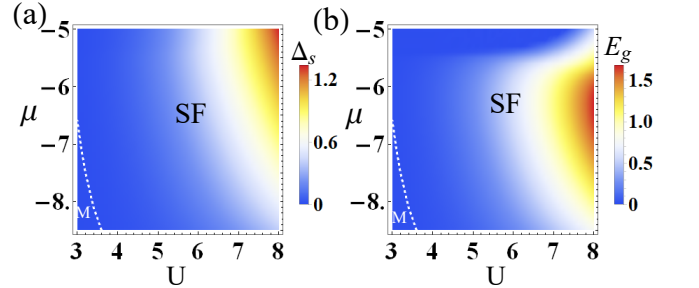


FIG. 2: (a) SF order parameter Δ_s versus interaction U and chemical potential μ . A phase transition occurs between metal (M) and superfluid (SF) phases. (b) Similar as panel (a) but plotted with Bogliubov quasiparticle energy gap E_g . In both panels, we take $t_x = t_y = 1$, $t_{sox} = t_{soy} = 2$, $h_z = 1.4$.

where $t_x = t_0 \cos(k_0 \cos \theta)$, $t_y = t_0 \cos(k_0 \sin \theta)$, $t_{sox} = t_0 \sin(k_0 \cos \theta)$, $t_{soy} = t_0 \sin(k_0 \sin \theta)$, and the bare hopping strength reads $t_0 = -\int d\vec{r} \psi_\sigma^*(\vec{r} - \vec{r}_i) \left(\frac{k_x^2 + k_y^2}{2m_0} + V_{\text{lat}} \right) \psi_\sigma(\vec{r} - \vec{r}_{i+1})$. Here, we have chosen the basis $\hat{c}_i = (\hat{c}_{i,\uparrow}, \hat{c}_{i,\downarrow})^T$ and denoted $h_z = \Omega$. The incident angle θ is illustrated in Fig. 1. The lattice spacing is set to be $a = 1$. Hereafter, we set $t_0 = 1/\cos[k_0 \sin(\pi/4)] = 1/\cos(\sqrt{2}\pi/4)$ for convenience. When $\theta = \pi/4$, we have approximately $t_{sox} = t_{soy} \approx 2t_x = 2t_y$.

We consider an attractive SU(2)-invariant interaction $\hat{H}_{int} = -\sum_i U \hat{n}_{i,\uparrow} \hat{n}_{i,\downarrow}$ and study the superfluid phase

under mean-field approach by solving the s -wave superfluid order parameter $\Delta_s = U \langle c_{i,\downarrow} c_{i,\uparrow} \rangle$ self-consistently. The Bogoliubov de Gennes (BdG) Hamiltonian in the Nambu basis $\Psi_k = (c_{k\uparrow}, c_{k\downarrow}, c_{-k\downarrow}^\dagger, -c_{-k\uparrow}^\dagger)^T$ is described by $\hat{H}_s = \sum_k \Psi_k^\dagger H(k) \Psi_k$ with

$$H(k) = (\epsilon_k + \gamma_k \sigma_y) \tau_z - h_z \sigma_z + \Delta_s \tau_x, \quad (3)$$

where $\epsilon_k = -2(t_x \cos k_x + t_y \cos k_y) - \mu$, $\gamma_k = 2(t_{sox} \sin k_x + t_{soy} \sin k_y)$, σ and τ are Pauli matrices acting on the spin and particle-hole spaces, respectively. By minimizing free energy with respect to the order parameter Δ_s and chemical potential μ , we may derive the following self-consistent equations

$$1 = \frac{U}{2N_l} \sum_{\nu=\pm, k} \frac{\tanh(\beta \xi_{k,\nu}/2)}{\xi_{k,\nu}} \left(1 + \frac{\nu h_z^2}{g_k}\right), \quad (4)$$

$$n_f = 1 - \frac{1}{N_l} \sum_{\nu=\pm, k} \epsilon_k \frac{\tanh(\beta \xi_{k,\nu}/2)}{\xi_{k,\nu}} \left(1 + \frac{\nu m_k^2}{g_k}\right) \quad (5)$$

where n_f is the particle filling factor, N_l is the number of lattice sites, and other parameters are defined as $\beta = 1/(k_B T)$ with k_B the Boltzmann constant and T the temperature, $\xi_{k,\nu=\pm} = \sqrt{\epsilon_k^2 + \Delta_s^2 + m_k^2 + 2\nu g_k}$, $g_k = \sqrt{\epsilon_k^2 m_k^2 + \Delta_s^2 h_z^2}$, and $m_k = \sqrt{h_z^2 + |\gamma_k|^2}$. By numerically solving equations (4) and (5), we obtain phase diagrams at zero temperature for pairing order Δ_s and quasiparticle energy gap E_g in Fig. 2 (a) and (b), respectively. Fig. 2 (a) confirms the phase transition from a metal (M) phase to an s -wave SF. From panel (b), we find a finite gap for Bogoliubov quasiparticle excitations in proper parameter region in the SF phase. The energy gap also survives on a finite-size sample and could protect Majorana modes from lower extended states.

III. MAJORANA CORNER PAIRS ON A TOPOLOGICAL DEFECTIVE RECTANGULAR GEOMETRY

Given a proper local dip potential, the defect chain enjoys a non-trivial topology, belonging to the BDI class. It can be characterized through a winding number, which is discussed in Appendix A. Similarly, with a local dip μ_d , we can get a defect rectangle in the 2D optical lattice as illustrated in Fig. 1, where SOC domain walls (anticlockwise or clockwise) naturally arise at two corners. In the following, we will first focus on the continuum limit to explore the nature of the emerged Majorana pairs, supplemented with self-consistent numerical calculations on a 2D optical lattice.

We assume that with appropriate μ_d , the defect rectangle enters the TSF phase while the rest part remains trivial. As a result, we could assume that the topological defect rectangle is isolated from the 2D bulk. The

numerics performed on a 2D optical lattice with an imprinted defect-rectangle also supports this assumption later. From Eq. (3), the low-energy Hamiltonian expands around $\vec{k} = (0, 0)$ on edges $m = \text{I, II, III, IV}$ (see Fig. 1) and is then given by

$$H_m = t_m k_m^2 \tau_z + 2t_{s,m} k_m \sigma_y \tau_z - \mu_m \tau_z - h_z \sigma_z + \Delta_{s,m} \tau_x, \quad (6)$$

where $t_{\text{I}} = t_{\text{III}} = t_y$, $t_{\text{II}} = t_{\text{IV}} = t_x$, $k_{\text{I}} = k_{\text{III}} = k_y$, $k_{\text{II}} = k_{\text{IV}} = k_x$, $t_{s,\text{I}} = t_{s,\text{III}} = 2t_{soy}$ and $t_{s,\text{II}} = t_{s,\text{IV}} = 2t_{sox}$. The on-site chemical potential is $\mu_m = \mu + 2(t_x + t_y) - \mu_d$ with μ_d the dip potential, and $\Delta_{s,m}$ the s -wave pairing on each edge. Without loss of generality, we set incident angle of Raman lasers $\theta = \frac{\pi}{4}$ such that $t_x = t_y = t$, $t_{sox} = t_{soy} = t_{so}$, $\mu_m = \mu_{\text{edge}} = \mu + 4t - \mu_d$, and assume the s -wave SF order parameter is nearly uniform on the four edges $\Delta_{s,m} = \Delta_{\text{edge}}$. For later convenience, we take an ‘‘edge coordinate’’ s , in which we take the anticlockwise direction as positive. In such a coordinate, the low-energy edge Hamiltonian reads

$$H_{\text{edge}} = -t\tau_z \frac{\partial^2}{\partial s^2} - i\alpha(s) \sigma_y \tau_z \frac{\partial}{\partial s} - \mu_{\text{edge}} \tau_z - h_z \sigma_z + \Delta_{\text{edge}} \tau_x, \quad (7)$$

with $\alpha(s) = -2t_{so}, 2t_{so}, 2t_{so}, -2t_{so}$ for edge I-IV respectively. Remarkably, while the terms Δ_{edge} and μ_{edge} remain the same on the four edges, the effective coupling $\alpha(s)$ changes sign at two of four corners (the corner between the edges I (III) and II (IV)), forming two SOC domain walls as illustrated in Fig. 1. This will give rise to a Majorana pair if $h_z^2 > \mu_{\text{edge}}^2 + \Delta_{\text{edge}}^2$. Specifically, at the corner between edge I and II (corner $s = 0$ in our coordinate), two orthogonal wave functions for MCMs are given by

$$\Psi_{0,\pm} = C_{\pm} e^{-\eta_{\pm}|s|} \left(e^{i\frac{\phi_{\pm}}{2}} |y_{+}\rangle_{\sigma} |y_{\pm}\rangle_{\tau} + e^{-i\frac{\phi_{\pm}}{2}} |y_{-}\rangle_{\sigma} |y_{\mp}\rangle_{\tau} \right). \quad (8)$$

Here, C_{\pm} are normalization constants and $e^{i\phi_{\pm}} = \frac{h_z [i(\alpha\eta_{\pm} \mp \Delta_{\text{edge}}) - (t\eta_{\pm}^2 + \mu_{\text{edge}})]}{(t\eta_{\pm}^2 + \mu_{\text{edge}})^2 + (\alpha\eta_{\pm} \mp \Delta_{\text{edge}})^2}$, where $\eta_{\pm} = \frac{1}{2} \sqrt{-\frac{2\kappa}{3} + \delta} \mp \frac{1}{2} \sqrt{-\frac{4\kappa}{3a} - \delta + \zeta_{\pm}} > 0$, $\zeta_{\pm} = \mp 2d / (a\sqrt{-2c/(3a)} + \delta)$, $\delta = \frac{\sqrt[3]{2}\delta_1}{3a\sqrt{\delta_2 + \sqrt{-4\delta_1^3 + \delta_2^2}}} + \frac{\sqrt[3]{\delta_2 + \sqrt{-4\delta_1^3 + \delta_2^2}}}{3\sqrt[3]{2}a}$, $\delta_1 = \kappa^2 + 12ae$, $\delta_2 = 2\kappa^3 + 27ad^2 - 72a\kappa e$, $a = t^2$, $\kappa = \alpha^2 + 2t\mu_{\text{edge}}$, $d = -2\alpha\Delta_{\text{edge}}$ and $e = \Delta_{\text{edge}}^2 - h_z^2 + \mu_{\text{edge}}^2$. The vectors $|y_{\pm}\rangle_{\sigma}$ and $|y_{\pm}\rangle_{\tau}$ are eigenstates of operators σ_y and τ_y , respectively. Following similar approach, we could also find two Majorana modes at the corner between edges III and IV (see Appendix B for details). We emphasize that as long as the four edges are in the TSF phase, the very existence of Majorana pairs is robust against the fluctuations of chemical potential and SF order parameter.

With the above understanding of continuum systems, we now proceed to study the discrete cases on an optical lattice shown in Fig. 1. The total Hamiltonian now

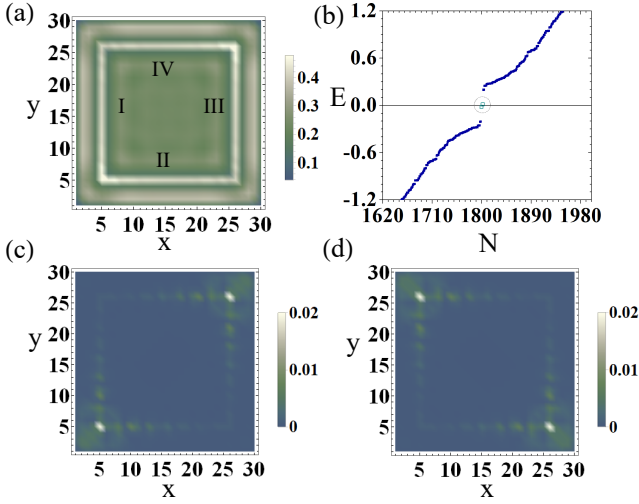


FIG. 3: (a) Self-consistent s -wave pairing order parameters in real space. (b) Energy level diagrams. (c,d) The real-space distributions of MZMs. For all panels, we choose $t_x = t_y = 1$, $t_{sox} = t_{soy} = 2$, $\mu = -7.95$, $\mu_d = -4.0$, $h = 1.4$, $U = 6.3$. The incident angle is $\theta = \pi/4$ in (a)-(c) and $\theta = -\pi/4$ in (d).

becomes

$$\hat{H}_{BdG} = \hat{H}_s + \sum_{i \in \square} \mu_d \hat{c}_i^\dagger \hat{c}_i, \quad (9)$$

where $i \in \square$ enumerate each site with the dip potential (a rectangular geometry in this case). The local s -wave superfluid order parameter in real space is determined in a self-consistent manner [15], as well as the quasiparticle energy spectra and wave functions. On the defect rectangle, the system is topological once $h_z > \sqrt{\tilde{\mu}^2 + \Delta_s^2}$ and $\tilde{\mu} = \mu + 2t_x + 2t_y - \mu_d$. In our self-consistent numerical calculations, we take the lattice sizes $n_x = n_y = 30$, and the defect rectangle is given by $n_x^d = n_y^d = 22$. The SF order parameter $\Delta_{s,i}$ is shown in Fig. 3 (a), which has a constant phase across the entire system. Fig. 3 (b) shows the quasiparticle energy spectrum, where four Majorana bound states (two Majorana corner pairs) exist in the energy gap. A small energy splitting is observed as a result of finite-size effect. Fig. 3 (c) shows the density distribution of the bounded Majorana corner states, which clearly demonstrates its localization at the corners of the defect rectangle. The Majorana corner pairs are robust against the perturbations of chemical potential and SF order parameter that preserve chiral symmetry. We have confirmed this point by numerical calculations.

The incident angle of Raman lasers can change the SOC and the nearest-neighbor hopping, and thus alter the Majorana bound states. Figs. 4 (a) and (b) illustrate the corresponding phase diagram with respect to μ - θ and μ_d - θ , where Majorana corner pairs exist in the topological region (T). It is found that the Majorana pairs is also robust to certain variation of the incident angle θ . We remark that if the sign of θ is reversed, the Majorana pairs appear at another two corners (the interfaces of II-III

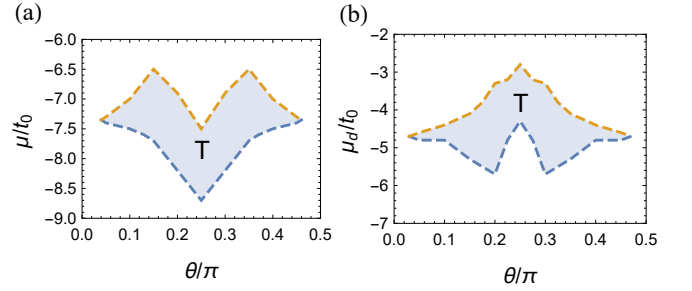


FIG. 4: Phase diagram for 2D system with the defect rectangle. In region ‘‘T’’, Majorana bound states exist at corners. In (a), $\mu_d = -4.0$, $h_z = 1.4$, $U = 6.3$ are used. In (b), $\mu = -7.8$, $h_z = 1.4$, $U = 6.3$ are used.

and I-IV) as shown in Fig. 3(d), which can be compared with Fig. 3(c). Thus, our proposed setup provides better tunability for manipulating Majorana bound states.

IV. MAJORANA CORNER PAIRS ON A RING GEOMETRY

In this section, we study the case with a ring-shaped defect line. Here, the optical lattice is removed and we focus on the low-energy effective 1D model for simplicity. The effective model is illustrated in Fig. 5 (a) and we find that soft domain walls of SOC naturally arise on the ring, which leads to the emergence of Majorana corner pairs.

Without loss of generality, we assume the momentum kick by Raman lasers is along the x direction. Under a spin-rotation $\sigma_y \rightarrow \sigma_x$ with $k_{0,y} = 0$ in Eq. (1), the SOC has the form $\alpha_0 k_x \sigma_x$, where the coupling constant is given by the ratio of laser wavevector and atomic mass, i.e., $\alpha_0 = k_0/m_0$. Hence, in the continuum limit, the effective Hamiltonian reads

$$\mathcal{H} = \frac{k^2}{2m_0} \tau_z + \alpha_0 k_x \sigma_x \tau_z - \mu \tau_z + h_z \sigma_z + \Delta_s \tau_x, \quad (10)$$

where Δ_s is an s -wave SF order. For simplicity, we set Δ_s to be real. The relation $h_z > \sqrt{\mu^2 + \Delta_s^2}$ holds in the topological regions.

In a polar coordinate (ρ, ϕ) , the above Hamiltonian becomes a function of polar angle ϕ on a ring with given radii ρ , i.e.,

$$\mathcal{H}(\phi) = -\eta \partial_\phi^2 \tau_z + i \tilde{\alpha}_0 \sin \phi \frac{\partial}{\partial \phi} \sigma_x \tau_z - \mu' \tau_z + h_z \sigma_z + \Delta_s \tau_x, \quad (11)$$

where $\eta = \frac{1}{2m_0 \rho^2}$, $\tilde{\alpha}_0 = \frac{\alpha_0}{\rho}$ and $\mu' = \mu - \frac{k_0^2}{2m_0}$ (more details are discussed in Appendix C). The Hamiltonian $\mathcal{H}(\phi)$ has particle-hole symmetry $\mathcal{P} \mathcal{H}(\phi) \mathcal{P}^{-1} = -\mathcal{H}(-\phi)$ where $\mathcal{P} = \sigma_y \tau_y \mathcal{K}$ and \mathcal{K} denotes the complex conjugation. It also preserves a generalized time-reversal symmetry $\mathcal{T} \mathcal{H}(\phi) \mathcal{T}^{-1} = \mathcal{H}(-\phi)$ with $\mathcal{T} = \sigma_z \mathcal{K}$. The combination of \mathcal{P} and \mathcal{T} leads to the chiral symmetry \mathcal{C} :

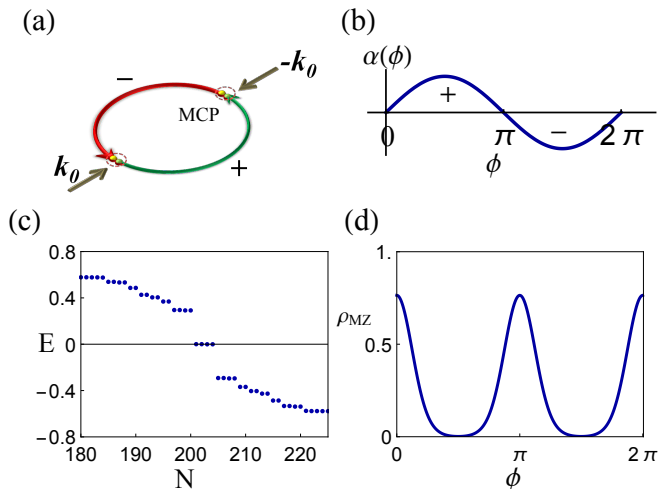


FIG. 5: (a) Illustration of a ring trap in which the atoms are confined. Two counter-propagating Raman lasers with wavevector $\pm \vec{k}_0$ couple the atomic hyperfine states. The notations + and - indicate the sign of SOC. Two spheres encircled by the red dashed circle denote a MCP. (b) The SOC term $\alpha(\phi)$ plotted to varying polar angle ϕ . (c) The eigenspectrum computed through plane-wave expansion. (d) The particle density ρ_{MZ} of Majorana zero modes versus the angle ϕ . The parameters are chosen as $\tilde{\alpha}_0 = 0.04$, $\eta = 0.005$, $\mu' = 0.2$, $h_z = -1.4$, $\Delta_s = 0.8$.

$\mathcal{C}\mathcal{H}(\phi)\mathcal{C}^{-1} = -\mathcal{H}(\phi)$, with $\mathcal{C} = \mathcal{PT} = i\sigma_x\tau_y$. Therefore, the Hamiltonian belongs to BDI class and can be characterized by a \mathbb{Z} topological invariant [56, 57].

In Eq. (11), the SOC $\alpha(\phi) = \tilde{\alpha}_0 \sin \phi$ changes sign at $\phi = 0, \pi$, as shown in Fig. 5 (b). Specifically, we have $\alpha(\phi) > 0$ if $\phi \in (0, \pi)$ and $\alpha(\phi) < 0$ if $\phi \in (\pi, 2\pi)$. Hence, the system can be divided into two segments. Both belong to the BDI class but possess opposite topological invariant. The interfaces are determined by $\phi = 0$ and π , corresponding to two “soft” domain walls in the sense that the SOC term changes smoothly across these two points. From Eq. (11), the Hamiltonian $\mathcal{H}(\phi)$ is invariant under a $2n\pi$ rotation if n is an integer. Therefore, to solve the eigenvalues of $\mathcal{H}(\phi)$, we assume the following trial solution,

$$\Phi(\phi) = (u_a(\phi), u_b(\phi), u_c(\phi), u_d(\phi))^T, \quad (12)$$

where $u_{\nu=a,b,c,d}(\phi) = \sum_m \nu_m e^{im\phi}$ and m is an integer. By solving the Schrödinger equation $\mathcal{H}(\phi)\Phi(\phi) = E\Phi(\phi)$, the eigenvalues are obtained as shown in Fig. 5 (c). See Appendix C for more details. It is clear that four Majorana modes emerge (with a numerical error about $E \approx 10^{-4}$). One Majorana corner pair consisting of two Majorana modes localizes at $\phi = 0$, and the other pair localizes at $\phi = \pi$, as illustrated in Fig. 5 (a). This is also demonstrated by the particle density distribution ρ_{MZ} of Majorana modes, as shown in Fig. 5 (d). We remark that a toroidal Bose-Einstein condensate has been created in an all-optical trap [58]. We expect our scheme

could be reached with similar techniques and additional Raman lasers.

V. DISCUSSION AND CONCLUSION

From the effective low-energy theory of TSFs, it is well-known that Majorana modes would emerge if the sign of the Dirac mass changes and most previous proposals are based on this principle. In this paper, we propose an alternative approach to implement Majorana modes (Majorana corner pairs) through tuning the effective SOC. By loading Fermi gases on 2D optical lattices subjected to a 1D ERD SOC, we can find a SF phase under appropriate s -wave interaction and Zeeman field. Using single-site addressing techniques, we could engineer defective geometries, which are topologically non-trivial, on the 2D optical lattice. From the viewpoint of low-energy theories, a defect rectangle consists of two TSFs characterized by distinct topological invariants whose sign is determined by the sign of SOC in edge coordinate. Obviously, the sign of SOC changes at two corners on the defect rectangle. At the interface of two distinct TSF, a topologically protected Majorana pair naturally arises according to the index theorem. For TSF with 1D ERD SOC on a ring, two soft SOC domain walls exist, and two Majorana pairs also appear near the domain walls. In principle, as long as two effective 1D SFs are topological with different topological invariants $w = \pm 1$, the Majorana pair will emerge at the interface. It is robust as long as the perturbations preserve three underlying symmetries (\mathcal{P} , \mathcal{T} , \mathcal{C}) of the system.

We emphasize that the Majorana corner pair in the context differs from those in second order TSCs in two dimensions. First, for second order TSCs with time reversal symmetry [42, 43], 1D edge modes evolve from the higher-dimensional bulk of the topological insulators. However, in our scheme, the 1D modes originate from the defect geometry. Second, in a higher-order TSC, a momentum-dependent SC pairing (s_{\pm} or d -wave) leads to Dirac mass kink at the corner of the sample, and then induces the Majorana Kramers pair. In contrary, our proposal utilizes the sign reverse of effective SOC on the edges and lacks Kramers degeneracy.

In summary, we propose a distinct scheme to implement Majorana pairs in an atomic platform. The coordinate of Majorana pair depends on the position of SOC domain wall which can be tuned by the directions of the Raman laser beams. Moreover, our system is free of dynamical instability such that the MZM has a longer lifetime. Our work opens the possibility of implementing robust Majorana pairs and the associated non-Abelian braiding in cold atoms.

Acknowledgments

This work is supported by Air Force Office of Scientific Research (FA9550-16-1-0387), National Science Foundation (PHY-1806227), and Army Research Office (W911NF-17-1-0128). This work is also supported in part by NSFC under the grant No. 11504285, and the Scientific Research Program Funded by Natural Science Basic Research Plan in Shaanxi Province of China (Program Nos. 2018JQ1058), the Scientific Research Program Funded by Shaanxi Provincial Education Department under the grant No. 18JK0397, and the scholarship from China Scholarship Council (CSC) (Program No. 201708615072).

Appendix A: Majorana modes at the ends of topological defect-chain

In this section, we show a topologically non-trivial defective chain can be implemented through on-site potential engineering on 2D optical lattices.

For a 1D system with SOC and SF order, the system is topological if $h_z > \sqrt{(\tilde{\mu} - \mu_d)^2 + \Delta_s^2}$, where $\tilde{\mu} = \mu + 2t_x + 2t_y$ [13–16]. Reference [15] shows Majorana fermions may be generated in a 2D optical lattices with 1D ERD SOC along the x direction. This motivates us to demonstrate the existence of Majorana bound states in a genuine 2D systems with 1D defects, where the SOC lays along $\vec{e}_x + \vec{e}_y$ direction. Through single-site addressing, a potential could be locally applied to a given site.

Imposing a 1D potential dip μ_d , we have the following Hamiltonian

$$\hat{H}_{BdG} = \hat{H}_s + \sum_{i \in -} \mu_d \hat{c}_i^\dagger \hat{c}_i, \quad (\text{A1})$$

where $i \in -$ denotes the sites (i_x, i_y) satisfying $i_y = n_{y_c}$. In self-consistent numerical calculations, we take a lattice with $n_x = 100$, $n_y = 9$ and $n_{y_c} = 5$ under open boundary conditions, where n_x and n_y denote the site number along the x and y directions. Figs. 6 (a) and (b) present self-consistent numerical results. Fig. 6 (b) shows density profile of the zero-energy mode ($E \approx 10^{-4}$). It demonstrates the existence of MZMs even in a genuine 2D system. From self-consistent BdG numerical results, the SF order parameter is almost homogeneous along the x direction as shown in Fig. 6 (a). Thus, with periodic boundary condition, the system has a translation symmetry along the x direction so that momentum k_x is a good quantum number. The 2D optical lattice can be regarded as layered 1D chain with transverse tunneling and SOC effects. The effective Hamiltonian is then written as

$$H_{BdG}(k_x) = \kappa_0 h_0(k_x) + \mu_d \kappa_c \sigma_0 \tau_z + \Delta_a \kappa_c \sigma_y \tau_y - t_y \kappa_x \sigma_0 \tau_z - t_{soy} \kappa_y \sigma_y \tau_z. \quad (\text{A2})$$

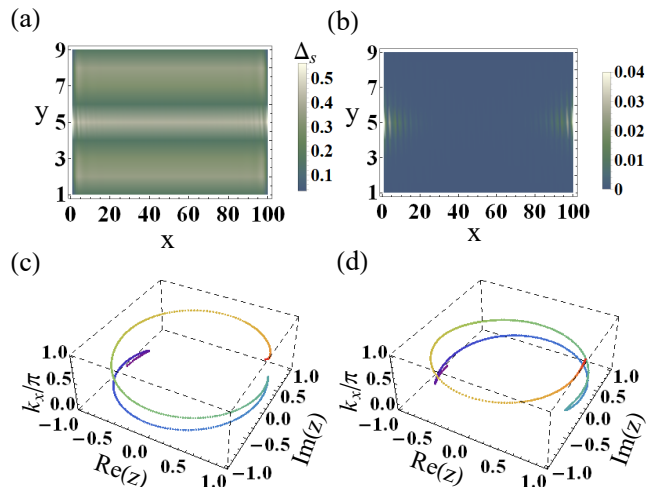


FIG. 6: (a) The amplitude of SF order parameter in real space. (b) The density distribution of the MZM. (c,d) $z(k_x)$ in the complex plane for opposite winding number. In all panels, we set $t_x = t_y = 1$, $h_z = 1.4$, $\mu = -8.0$, $\mu_d = -4$, $\Delta_s = 0.3$ and $\Delta_a = 0.11$. We choose $t_{sox} = t_{soy} = 2$ in (a-c) and $t_{sox} = t_{soy} = -2$ in (d).

Here, the matrix κ acts on chain space, with κ_0 identity matrix, $(\kappa_c)_{i,i} = 1$ for $i = n_{y_c}$ and 0 otherwise, $(\kappa_x)_{i,j} = 1$ for $|i - j| = 1$ and $(\kappa_y)_{i,i \mp 1} = \mp i$ and 0 otherwise. The term proportional to μ_d (Δ_a) describes the dip potential (the SF-order) difference between the central chain and other individual chains. The term proportional to t_y (t_{soy}) describes the hopping (SOC) along the y direction. The following Hamiltonian

$$h_0(k_x) = (-2t_x \cos k_x - \mu) \sigma_0 \tau_z + 2t_{sox} \sin k_x \sigma_y \tau_z + h_z \sigma_z \tau_z + \Delta_s \sigma_y \tau_y \quad (\text{A3})$$

describes the original uniform individual 1D chain along the x direction. σ and τ are Pauli matrices acting on spin space and particle-hole space, respectively. The above BdG Hamiltonian $H_{BdG}(k_x)$ has intrinsic particle-hole symmetry \mathcal{P} : $\mathcal{P} H_{BdG}(k_x) \mathcal{P}^{-1} = -H_{BdG}(-k_x)$ with $\mathcal{P} = \tilde{\tau}_x \mathcal{K}$, $\tilde{\tau}_x = \tau_x \sigma_0 \eta_0$, where σ_0 is 2×2 identity matrix, η_0 is a $N_s \times N_s$ identity matrix acting on the lattice site space, and \mathcal{K} is the complex conjugation. If the superfluid order parameter is real (or has a constant phase that can be eliminated by gauge transformations), the Hamiltonian preserves a generalized time-reversal symmetry \mathcal{T} : $\mathcal{T} H_{BdG}(k_x) \mathcal{T}^{-1} = H_{BdG}(-k_x)$ with $\mathcal{T} = \mathcal{K}$. The composite operation of \mathcal{P} and \mathcal{T} also leads to a chiral symmetry \mathcal{C} : $\mathcal{C} H_{BdG}(k_x) \mathcal{C}^{-1} = -H_{BdG}(k_x)$, with $\mathcal{C} = \mathcal{P} \mathcal{T} = \tilde{\tau}_x$. From above symmetry analyses, the Hamiltonian belongs to BDI class, characterized by a \mathbb{Z} topological invariant (winding number).

The winding number w can characterize the topological properties of BdG Hamiltonian (A2) [17]. Because the BdG Hamiltonian H_{BdG} has the chiral symmetry, it can be transformed into an off-diagonal form in particle-

hole space under a unitary transformation $U = e^{-i\frac{\pi}{4}\tau_y}$,

$$UH_{BdG}(k_x)U^{-1} = \begin{pmatrix} 0 & \mathcal{B}(k_x) \\ \mathcal{B}^T(-k_x) & 0 \end{pmatrix}. \quad (\text{A4})$$

Here, $\mathcal{B}(k_x) = \mathcal{B}_1(k_x) - i\mathcal{B}_2$, where $\mathcal{B}_1(k_x) = (-2t_x \cos k_x - \mu) \kappa_0 \sigma_0 + 2t_{sox} \sin k_x \kappa_0 \sigma_y + h_z \kappa_0 \sigma_z + \mu_d \kappa_c \sigma_0 - t_y \kappa_x \sigma_0 - t_{soy} \kappa_y \sigma_y$ and $\mathcal{B}_2 = (\Delta_s \kappa_0 \sigma_y + \Delta_a \kappa_c \sigma_y)$. The winding number is defined as [17]

$$w = -\frac{i}{\pi} \int_0^\pi \frac{dz}{z(k_x)}, \quad (\text{A5})$$

where $z(k_x) = \det(\mathcal{B}(k_x)) / |\det(\mathcal{B}(k_x))|$. As shown in Figs. 6 (c) and (d) with $h_z > \sqrt{(\mu + 2t_x + 2t_y - \mu_d)^2 + \Delta_s^2}$, the complex value of $z(k_x)$ varies when k_x changes from 0 to π , indicating $|w| = 1$. By considering the trajectory of $z(k_x)$ in the complex plane as k_x changing from 0 to π , $z(k_x)$ moves from a point on the negatively real axis to the positive axis while crossing the imaginary axis exactly once. It is clear that the winding number $w = -1$ when $t_{sox} > 0$ in topological phase, as shown in Fig. 6 (c), and the winding number $w = +1$ when $t_{sox} < 0$ in topological phase, as shown in Fig. 6 (d). Namely, the sign of winding number for the defect chain is determined by the sign of SOC in the topological phase.

Appendix B: Low-energy theory of topological superfluids on a defective rectangle

Remarkably, from Eq. (7) the term Δ_{edge} doesn't change sign, but the coefficient $\alpha(s)$ changes sign at two corners of defect-rectangle. This will give rise to a Majorana pair at the corner where $\alpha(s)$ changes sign. Hereafter, we will give the analytic solutions of Majorana corner modes.

According to the particle-hole symmetry of H_{edge} , i.e., $\{H_{\text{edge}}, \sigma_y \tau_y\} = 0$, we have

$$H_{\text{edge}} \sigma_y \tau_y = -\sigma_y \tau_y H_{\text{edge}}. \quad (\text{B1})$$

It can be concluded that if there exist zero-energy states of H_{edge} , these states are also eigenstates of $\sigma_y \tau_y$. Therefore, we assume the zero-energy wave functions in the "edge coordinate" s have the following forms:

$$\Psi_{0,+} = f_+(s) |y_+\rangle_\sigma |y_+\rangle_\tau + g_+(s) |y_-\rangle_\sigma |y_-\rangle_\tau, \quad (\text{B2})$$

$$\Psi_{0,-} = f_-(s) |y_+\rangle_\sigma |y_-\rangle_\tau + g_-(s) |y_-\rangle_\sigma |y_+\rangle_\tau. \quad (\text{B3})$$

Then we have $\sigma_y \tau_y \Psi_{0,\pm} = \pm \Psi_{0,\pm}$ and the Schrödinger equation at the corner between the edge I and II (corner $s = 0$) is $H_{\text{edge}} \Psi_{0,+} = 0$. Using the eigenvector $\Phi = (f_+(s), g_+(s))^T$, the above equation (B1) can be rewritten as

$$(t\partial_s^2 + i\alpha\partial_s\sigma_z + \mu_{\text{edge}} - i\Delta_{\text{edge}}\sigma_z + h_z\sigma_x) \Phi = 0. \quad (\text{B4})$$

We assume $f_+(s) = A_+ e^{-\eta_+ s}$, $g_+(s) = B_+ e^{-\eta_+ s}$ ($s > 0$) and write

$$(-it\eta_+^2\sigma_z + \alpha\eta_+ - i\mu_{\text{edge}}\sigma_z - \Delta_{\text{edge}} + h_z\sigma_y) \tilde{\Phi} = 0, \quad (\text{B5})$$

with $\tilde{\Phi} = (A_+, B_+)^T$. According to the vanishing determinant of the above matrix, we obtain

$$\eta_+ = \frac{1}{2} \sqrt{-\frac{2\kappa}{3} + \delta} - \frac{1}{2} \sqrt{-\frac{4\kappa}{3a} - \delta + \zeta_+} > 0, \quad (\text{B6})$$

where κ , δ , a , and ζ_+ have been written explicitly in the main text. Then we have $A_+/B_+ = e^{i\phi_+}$ with

$$e^{i\phi_+} = \frac{h_z [-(t\eta_+^2 + \mu_{\text{edge}}) + i(\alpha\eta_+ - \Delta_{\text{edge}})]}{(t\eta_+^2 + \mu_{\text{edge}})^2 + (\alpha\eta_+ - \Delta_{\text{edge}})^2}. \quad (\text{B7})$$

At last, we get the MZM $\Psi_{0,+}$ at the corner between the edge I and II. Following similar approach as in previous calculations, we can get another zero energy solution $\Psi_{0,-} = C_- e^{-\eta_- |s|} (e^{i\frac{\phi_-}{2}} |y_+\rangle_\sigma \otimes |y_-\rangle_\tau + e^{-i\frac{\phi_-}{2}} |y_-\rangle_\sigma \otimes |y_+\rangle_\tau)$ with C_- the normalization constant, where

$$\eta_- = \frac{1}{2} \sqrt{-\frac{2\kappa}{3} + \delta} + \frac{1}{2} \sqrt{-\frac{4\kappa}{3a} - \delta + \zeta_-} > 0, \quad (\text{B8})$$

$$e^{i\phi_-} = \frac{h_z [-(t\eta_-^2 + \mu_{\text{edge}}) + i(\alpha\eta_- + \Delta_{\text{edge}})]}{(t\eta_-^2 + \mu_{\text{edge}})^2 + (\alpha\eta_- + \Delta_{\text{edge}})^2}. \quad (\text{B9})$$

and the coefficients κ , δ , a and ζ_- are listed in the main text. In summary, there are two Majorana modes (a Majorana corner pair) localized around the corner with analytic solution given in Eq. (8). Regarding the corner between III and IV, there exists another SOC domain wall and we similarly have a Majorana pair there.

Appendix C: Low-energy theory of topological superfluids on a defective ring

The general Hamiltonian for a SOC fermi gas with Cooper pairing is given by

$$H_r = \frac{1}{2m_0} (\vec{k} - k_0 \vec{\sigma})^2 - \mu\tau_z + h_z\sigma_z + \Delta_s\tau_x, \quad (\text{C1})$$

where $\vec{k} = -i\vec{\nabla}$. Assuming spin $\vec{\sigma}$ is along x and neglecting the constant energy shift $k_0^2/(2m_0)$, we get the Hamiltonian in Eq. (10). In the polar coordinate,

$$\begin{pmatrix} \vec{i} \\ \vec{j} \end{pmatrix} = \begin{pmatrix} \cos \phi & -\sin \phi \\ \sin \phi & \cos \phi \end{pmatrix} \begin{pmatrix} \vec{e}_\rho \\ \vec{e}_\varphi \end{pmatrix}. \quad (\text{C2})$$

The Laplace operator in Descartes and polar coordinates is written as

$$\vec{\nabla} = \partial_x \vec{i} + \partial_y \vec{j} = \partial_\rho \vec{e}_\rho + \frac{1}{\rho} \partial_\phi \vec{e}_\phi. \quad (\text{C3})$$

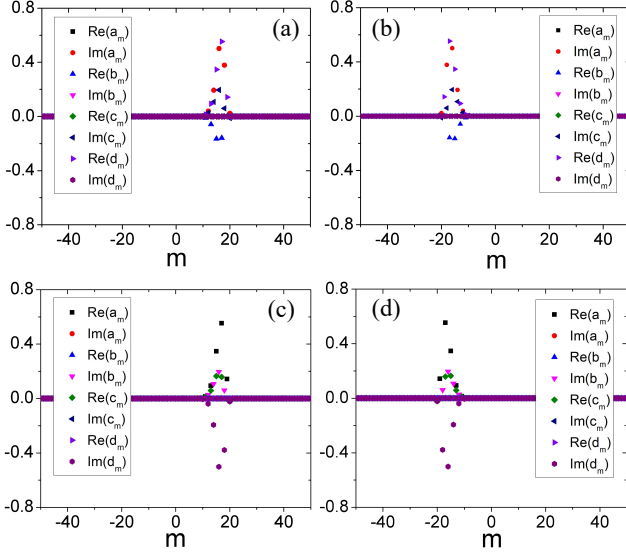


FIG. 7: The real and imaginary parts of coefficients (a_m, b_m, c_m, d_m) for the wave functions of four Majorana modes, respectively. Parameters $\tilde{\alpha}_0 = 0.04$, $\eta = 0.005$, $\mu' = 0.2$, $h_z = -1.4$, $\Delta = 0.8$ are used for all panels.

Then we have $\vec{k}^2 = -\vec{\nabla} \cdot \vec{\nabla} = -\left(\partial_\rho^2 + \frac{1}{\rho^2}\partial_\phi^2\right)$ and

$$\vec{k} \cdot (\sigma_x \vec{i}) = -i \left[\cos \phi \partial_\rho + \frac{1}{\rho} \partial_\phi (-\sin \phi) \right] \sigma_x. \quad (\text{C4})$$

Finally, Eq. (10) can be rewritten as the following form:

$$\begin{aligned} \mathcal{H} = & \frac{1}{2m_0} \left[-\left(\partial_\rho^2 + \frac{1}{\rho^2}\partial_\phi^2\right) - ik_0 \left(\cos \phi \partial_\rho - \frac{1}{\rho} \sin \phi \partial_\phi \right) \right. \\ & \times \sigma_x - ik_0 \left(\cos \phi \partial_\rho - \frac{1}{\rho} \sin \phi \partial_\phi \right) \sigma_x \left. \right] \tau_z - \mu \tau_z \\ & + h_z \sigma_z + \Delta_s \tau_x. \end{aligned} \quad (\text{C5})$$

Consider ultracold atoms trapped in a ring-shaped trapping potential, where the radii ρ is fixed. Terms with respect to ∂_ρ disappear. After substituting $\eta = \frac{1}{2m_0\rho^2}$, $\tilde{\alpha}_0 = \frac{k_0}{m_0\rho} = \frac{\alpha_0}{\rho}$, and $\mu' = \mu - \frac{k_0^2}{2m_0}$, the Hamiltonian \mathcal{H} becomes Eq. (11).

Because $\mathcal{H}(\phi)$ is invariant under a $2n\pi$ rotation with n being an integer, we assume the wave functions take following form as $\Phi(\phi) = (u_a(\phi), u_b(\phi), u_c(\phi), u_d(\phi))^T$, where $u_{\nu=a,b,c,d}(\phi) = \sum_{m=-N}^N \nu_m e^{im\phi}$. Plugging $\mathcal{H}(\phi)$ and $\Phi(\phi)$ into the Schrödinger equation $\mathcal{H}\Phi(\phi) = E\Phi(\phi)$, and matching coefficients for $e^{im\phi}$, one can obtain a series of coupled equations as

$$\begin{aligned} E a_m = & (\eta^2 m^2 - \mu' + h_z) a_m + i \frac{\tilde{\alpha}_0}{2} (m-1) b_{m-1} \\ & - i \frac{\tilde{\alpha}_0}{2} (m+1) b_{m+1} + \Delta_s c_m, \end{aligned} \quad (\text{C6})$$

$$\begin{aligned} E b_m = & i \frac{\tilde{\alpha}_0}{2} (m-1) a_{m-1} - i \frac{\tilde{\alpha}_0}{2} [m+1] a_{m+1} \\ & + (\eta m^2 - \mu' - h_z) b_m + \Delta_s d_m, \end{aligned} \quad (\text{C7})$$

$$\begin{aligned} E c_m = & \Delta_s a_m + [-\eta m^2 + \mu' + h_z] c_m - i \frac{\tilde{\alpha}_0}{2} (m-1) d_{m-1} \\ & + i \frac{\tilde{\alpha}_0}{2} (m+1) d_{m+1}, \end{aligned} \quad (\text{C8})$$

$$\begin{aligned} E d_m = & \Delta_s b_m - i \frac{\tilde{\alpha}_0}{2} (m-1) c_{m-1} + i \frac{\tilde{\alpha}_0}{2} (m+1) c_{m+1} \\ & + [-\eta m^2 + \mu' - h_z] d_m. \end{aligned} \quad (\text{C9})$$

By solving above coupled equations (C6)-(C9) with the truncation bounds for m up to 50, the eigenenergies and corresponding eigenfunctions $\Phi(\phi)$ could be obtained. Fig. 5 (c) in the main text presents the eigenspectrum, indicating that there are four Majorana zero modes. The coefficients ν_m of wavefunctions of four Majorana modes are plotted in Fig. 7.

-
- [1] C. Nayak, S. H. Simon, A. Stern, M. Freedman, and S. Das Sarma, Non-Abelian anyons and topological quantum computation, *Rev. Mod. Phys.* **80**, 1083 (2008).
- [2] A. Y. Kitaev, Fault-tolerant quantum computation by anyons, *Ann. Phys.* **303**, 2 (2003).
- [3] S. R. Elliott and M. Franz, Majorana fermions in nuclear, particle, and solid-state physics, *Rev. Mod. Phys.* **87**, 137 (2015).
- [4] N. Read and D. Green, Paired states of fermions in two dimensions with breaking of parity and time-reversal symmetries and the fractional quantum Hall effect, *Phys. Rev. B* **61**, 10267 (2000).
- [5] V. T. Phong, N. R. Walet, and F. Guinea, Majorana zero modes in a two-dimensional p -wave superconductor, *Phys. Rev. B* **96**, 060505(R) (2017).
- [6] X.-L. Qi and S.-C. Zhang, Topological insulators and superconductors, *Rev. Mod. Phys.* **83**, 1057 (2011).
- [7] M. Z. Hasan and C. L. Kane, Colloquium: Topological insulators, *Rev. Mod. Phys.* **82**, 3045 (2010).
- [8] M. Sato, Y. Takahashi, and S. Fujimoto, Non-Abelian topological order in s -wave superfluids of ultracold fermionic atoms, *Phys. Rev. Lett.* **103**, 020401 (2009).
- [9] C. Zhang, S. Tewari, R. M. Lutchyn, and S. Das Sarma, $p_x + ip_y$ superfluid from s -wave interactions of fermionic cold atoms, *Phys. Rev. Lett.* **101**, 160401 (2008).
- [10] L. Jiang, T. Kitagawa, J. Alicea, A. R. Akhmerov, D. Pekker, G. Refael, J. I. Cirac, E. Demler, M. D. Lukin, and P. Zoller, Majorana fermions in equilibrium and in driven cold-atom quantum chains, *Phys. Rev. Lett.* **106**, 220402 (2011).
- [11] J. Alicea, Y. Oreg, G. Refael, F. von Oppen, and M. P. A. Fisher, Non-Abelian statistics and topological quantum information processing in 1D chain networks, *Nat. Phys.* **7**, 412 (2011).

- [12] J. Alicea, New directions in the pursuit of Majorana fermions in solid state systems, *Rep. Prog. Phys.* **75**, 076501 (2012).
- [13] Y. Oreg, G. Refael, and F. von Oppen, Helical Liquids and Majorana Bound States in Quantum Wires, *Phys. Rev. Lett.* **105**, 177002 (2010).
- [14] R. M. Lutchyn, J. D. Sau, and S. Das Sarma, Majorana Fermions and a Topological Phase Transition in Semiconductor-Superconductor Heterostructures, *Phys. Rev. Lett.* **105**, 077001 (2010).
- [15] L. Jiang, C. Qu, and C. Zhang, One-dimensional topological chains with Majorana fermions in two-dimensional nontopological optical lattices, *Phys. Rev. A* **93**, 063614 (2016).
- [16] J. D. Sau, R. M. Lutchyn, S. Tewari, and S. Das Sarma, Generic New Platform for Topological Quantum Computation Using Semiconductor Heterostructures, *Phys. Rev. Lett.* **104**, 040502 (2010).
- [17] S. Tewari and J. D. Sau, Topological Invariants for Spin-Orbit Coupled Superconductor Nanowires, *Phys. Rev. Lett.* **109**, 150408 (2012).
- [18] T. Ojanen, Topological π Josephson junction in superconducting Rashba wires, *Phys. Rev. B* **87**, 100506 (2013).
- [19] V. Mourik, K. Zuo, S. M. Frolov, S. Plissard, E. Bakkers, and L. Kouwenhoven, Signatures of majorana fermions in hybrid superconductor-semiconductor nanowire devices, *Science* **336**, 1003 (2012).
- [20] A. D. K. Finck, D. J. Van Harlingen, P. K. Mohseni, K. Jung, and X. Li, Anomalous modulation of a zero bias peak in a hybrid nanowire-superconductor device, *Phys. Rev. Lett.* **110**, 126406 (2013).
- [21] S. Nadj-Perge, I. K. Drozdov, J. Li, H. Chen, S. Jeon, J. Seo, A. H. MacDonald, B. A. Bernevig, and A. Yazdani, Observation of majorana fermions in ferromagnetic atomic chains on a superconductor, *Science* **346**, 602 (2014).
- [22] J.-P. Xu, M.-X. Wang, Z. L. Liu, J.-F. Ge, X. Yang, C. Liu, Z. A. Xu, D. Guan, C. L. Gao, D. Qian, Y. Liu, Q.-H. Wang, F.-C. Zhang, Q.-K. Xue, and J.-F. Jia, Experimental detection of a majorana mode in the core of a magnetic vortex inside a topological insulator-superconductor $\text{Bi}_2\text{Te}_3/\text{NbSe}_2$ heterostructure, *Phys. Rev. Lett.* **114**, 017001 (2015).
- [23] Z. F. Wang, H. Zhang, D. Liu, C. Liu, C. Tang, C. Song, Y. Zhong, J. Peng, F. Li, C. Nie, L. Wang, X. J. Zhou, X. Ma, Q. K. Xue, and F. Liu, Topological edge states in a high-temperature superconductor $\text{FeSe}/\text{SrTiO}_3$ (001) film, *Nat. Materials* **15**, 968 (2016).
- [24] Q. L. He, L. Pan, A. L. Stern, E. Burks, X. Che, G. Yin, J. Wang, B. Lian, Q. Zhou, E. S. Choi, K. Murata, X. Kou, T. Nie, Q. Shao, Y. Fan, S.-C. Zhang, K. Liu, J. Xia, and K. L. Wang, Chiral Majorana edge state in a quantum anomalous Hall insulator-superconductor structure, *Science* **357**, 294 (2017).
- [25] Y.-J. Lin, K. Jiménez-García, and I.B. Spielman, Spin-orbit-coupled Bose-Einstein condensates, *Nature* **471**, 83(2011).
- [26] J.-Y. Zhang, S.-C. Ji, Z. Chen, L. Zhang, Z.-D. Du, B. Yan, G.-S. Pan, B. Zhao, Y.-J. Deng, H. Zhai, S. Chen, and J.-W. Pan, Collective dipole oscillations of a spin-orbit coupled Bose-Einstein condensate, *Phys. Rev. Lett.* **109**, 115301 (2012).
- [27] P. Wang, Z.-Q. Yu, Z. Fu, J. Miao, L. Huang, S. Chai, H. Zhai, and J. Zhang, Spin-orbit coupled degenerate Fermi gases, *Phys. Rev. Lett.* **109**, 095301 (2012).
- [28] R. A. Williams, M. C. Beeler, L. J. LeBlanc, and I. B. Spielman, Raman-induced interactions in a single-component Fermi gas near an s -wave Feshbach resonance, *Phys. Rev. Lett.* **111**, 095301 (2013).
- [29] L. Huang, Z. Meng, P. Wang, P. Peng, S.-L. Zhang, L. Chen, D. Li, Q. Zhou, and J. Zhang, Experimental realization of two-dimensional synthetic spin-orbit coupling in ultracold Fermi gases, *Nat. Phys.* **12**, 540 (2016).
- [30] Z. Meng, L. Huang, P. Peng, D. Li, L. Chen, Y. Xu, C. Zhang, P. Wang, and J. Zhang, Experimental observation of a topological band gap opening in ultracold Fermi gases with two-dimensional spin-orbit coupling, *Phys. Rev. Lett.* **117**, 235304 (2016).
- [31] Z. Wu, L. Zhang, W. Sun, X.-T. Xu, B.-Z. Wang, S.-C. Ji, Y. Deng, S. Chen, X.-J. Liu, J.-W. Pan, Realization of two-dimensional spin-orbit coupling for Bose-Einstein condensates, *Science* **354**, 83 (2016).
- [32] A. Bühler, N. Lang, C. V. Kraus, G. Moller, S. D. Huber, H. P. Büchler, *Nat. Commun.* **5**, 4504 (2014).
- [33] D.-L. Deng, S.-T. Wang, K. Sun, and L.-M. Duan, Proposal for observing non-Abelian statistics of Majorana-Shockley fermions in an optical lattice, *Phys. Rev. B* **91**, 094513 (2015).
- [34] J. Langbehn, Y. Peng, L. Trifunovic, F. von Oppen, and P. W. Brouwer, Reflection-Symmetric Second-Order Topological Insulators and Superconductors, *Phys. Rev. Lett.* **119**, 246401 (2017).
- [35] W. A. Benalcazar, B. A. Bernevig, and T. L. Hughes, Quantized electric multipole insulators, *Science* **357**, 61 (2017).
- [36] Z. Song, Z. Fang, and C. Fang, $(d-2)$ -Dimensional Edge States of Rotation Symmetry Protected Topological States, *Phys. Rev. Lett.* **119**, 246402(2017).
- [37] C. Fang and L. Fu, Rotation Anomaly and Topological Crystalline Insulators, *arXiv:1709.01929*.
- [38] F. Schindler, A. M. Cook, M. G. Vergniory, Z. Wang, S. S. P. Parkin, B. A. Bernevig, T. Neupert, Higher-order topological insulators, *Sci. Adv.* **4**, eaat0346 (2018).
- [39] E. Khalaf, H. C. Po, A. Vishwanath, and H. Watanabe, Symmetry indicators and anomalous surface states of topological crystalline insulators, *Phys. Rev. X* **8**, 031070 (2018).
- [40] X. Zhu, Tunable Majorana corner states in a two-dimensional second-order topological superconductor induced by magnetic fields, *Phys. Rev. B* **97**, 205134 (2018).
- [41] E. Khalaf, Higher-order topological insulators and superconductors protected by inversion symmetry, *Phys. Rev. B* **97**, 205136 (2018).
- [42] Z. Yan, F. Song, and Z. Wang, Majorana Corner Modes in a High-Temperature Platform, *Phys. Rev. Lett.* **121**, 096803 (2018).
- [43] Q. Wang, C.-C. Liu, Y.-M. Lu, and F. Zhang, High-Temperature Majorana Corner States, *Phys. Rev. Lett.* **121**, 186801 (2018).
- [44] Y. Wang, M. Lin, and T.L. Hughes, Weak-Pairing Higher Order Topological Superconductors *Phys. Rev. B* **98**, 165144 (2018).
- [45] T. Liu, J. J. He, and F. Nori, Majorana corner states in a two-dimensional magnetic topological insulator on a high-temperature superconductor, *Phys. Rev. B* **98**, 245413 (2018).
- [46] C.-H. Hsu, P. Stano, J. Klinovaja, and D. Loss, Majorana

- rana Kramers pairs in higher-order topological insulators, *Phys. Rev. Lett.* **121**, 196801 (2018).
- [47] Y. Xu, L. Mao, B. Wu, and C. Zhang, Dark Solitons with Majorana Fermions in Spin-Orbit-Coupled Fermi Gases, *Phys. Rev. Lett.* **113**, 130404 (2014).
- [48] X.-J. Liu, Soliton-induced Majorana fermions in a one-dimensional atomic topological superfluid, *Phys. Rev. A* **91**, 023610 (2015).
- [49] P. Würtz, T. Langen, T. Gericke, A. Koglbauer, and H. Ott, Experimental demonstration of single-site addressability in a two-dimensional optical lattice. *Phys. Rev. Lett.* **103**, 080404 (2009).
- [50] W. S. Bakr, J. I. Gillen, A. Peng, S. Fölling, and M. Greiner, A quantum gas microscope for detecting single atoms in a Hubbard-regime optical lattice, *Nature* **462**, 74 (2009).
- [51] W. S. Bakr, A. Peng, M. E. Tai, R. Ma, J. Simon, J. I. Gillen, S. Foelling, L. Pollet, and M. Greiner, Probing the Superfluid-to-Mott Insulator Transition at the Single-Atom Level, *Science* **329**, 547 (2010).
- [52] J. F. Sherson, C. Weitenberg, M. Endres, M. Cheneau, I. Bloch, and S. Kuhr, Single-atom-resolved fluorescence imaging of an atomic Mott insulator, *Nature* **467**, 68 (2010).
- [53] C. Weitenberg, M. Endres, J. F. Sherson, M. Cheneau, P. Schauß, T. Fukuhara, I. Bloch, and S. Kuhr, Single-spin addressing in an atomic Mott insulator, *Nature* **471**, 319 (2011).
- [54] T. Köhler, K. Góral, and P. S. Julienne, Production of cold molecules via magnetically tunable Feshbach resonances, *Rev. Mod. Phys.* **78**, 1311 (2006).
- [55] C. Chin, R. Grimm, P. Julienne, and E. Tiesinga, Feshbach resonances in ultracold gases, *Rev. Mod. Phys.* **82**, 1225 (2010).
- [56] A. Altland and M. R. Zirnbauer, Nonstandard symmetry classes in mesoscopic normal-superconducting hybrid structures, *Phys. Rev. B* **55**, 1142 (1997).
- [57] A. P. Schnyder, S. Ryu, A. Furusaki, and A. W. W. Ludwig, Classification of topological insulators and superconductors in three spatial dimensions, *Phys. Rev. B* **78**, 195125 (2008).
- [58] A. Ramanathan, K. C. Wright, S. R. Muniz, M. Zelan, W. T. Hill III, C. J. Lobb, K. Helmerson, Superflow in a Toroidal Bose-Einstein Condensate: An Atom Circuit with a Tunable Weak Link, *Phys. Rev. Lett.* **106**, 130401 (2011).